Static Response of a Cylindrical Composite Panel with Cutouts Using a Geometrically Nonlinear Theory

S. T. Dennis* and A. N. Palazotto†
Air Force Institute of Technology, Wright-Patterson AFB, Ohio

A geometrically nonlinear static shell theory allowing large displacements and rotations and parabolic transverse shear is developed. The theory is cast into a total Lagrangian finite-element formulation for approximate solutions. The approach is then applied to the problem of an axially compressed quasiisotropic cylindrical shell panel with a cutout up to and beyond collapse. Analytical results compare very well with experimental findings for both global and local panel response.

I. Introduction

THE nonlinear behavior of axially compressed composite shell panels has been studied by several investigators.[1-15] However, the consideration of the geometric imperfection of a cutout in the shell structure has been studied primarily by NASA[4] and AFIT.[6,9,11,12,14] Analytical models using flat moderate rotation shell finite elements have been able to predict the panel response accurately except for geometries that have larger circular[4] and square[11] cutouts. The purpose of this paper is to apply a unique approach to composite cylindrical shell panels that have large cutouts. The approach includes several features of composite shell behavior. Through the thickness, parabolic transverse shear distribution is assumed similar to that proposed by Reddy.[16] Additionally, a simplified large rotation capability is included. The resulting finite element is cylindrically shaped, thus capturing shell bending-membrane coupling.

II. Theoretical Approach

Consider a shell geometry that can be described by orthogonal curvilinear middle surface coordinates, ξ_1 and ξ_2, surface normal ζ, and radii or curvature, R_1 and R_2, as shown in Fig. 1. A geometrically nonlinear theory governing the shell is based on the following assumptions:

1) The shell is thin and therefore assume that it is in an approximate state of plane stress, i.e., the transverse normal stress, $\sigma_3 \cong 0$. This assumption effectively reduces the generally three-dimensional behavior of the shell so that it can be described by the behavior of only a datum surface, this results in a two-dimensional approach.

2) The transverse shear-stress distribution is parabolic through the shell thickness and vanishes on the top and bottom surfaces of the shell.

Because the shell is thin, in-plane stresses tend to dominate the shell response, i.e., the transverse stresses are of lesser importance. However, it is well-known that laminated flat plates are significantly influenced by transverse shear deformation. Similar results have been found for laminated shells.[17,18] Therefore, transverse shear stresses are included in the present model, via a two-dimensional approach, whereas transverse normal stress is not. This approach is consistent with remarks made by Koiter[19] and John[20] who performed order-of-magnitude studies on the stresses in general shell structures. Additionally, their results are seen to hold approximately true in the linear elasticity solutions of both laminated flat plates by Pagano[21] and laminated shells in cylindrical bending by Ren.[22]

3) The shell is restricted to small strains and consists of linear elastic laminated orthotropic material .

4) Exact Green's strain-displacement relations are assumed for the in-plane strains, ϵ_1, ϵ_2, and ϵ_6, and linear strain-displacement relations are assumed for the transverse strains ϵ_4 and ϵ_5.

Librescu[17] developed a general shell equations based upon varying approximations in the magnitudes of both strain and the rotations differential elements undergo during deformation. A consistent small strain, *moderate* rotation theory has nonlinear (not exact) strain-displacement relations for the in-plane strains yet linear relations for the transverse shear strains. The present approach can therefore be viewed as a small strain, simplified large rotation theory due to the exact in-plane strain assumption together with the linear transverse strain assumption.

Kinematics

Following the developments in Ref. 18, let the kinematics of Eq. (1) represent the continuum displacements of the shell,

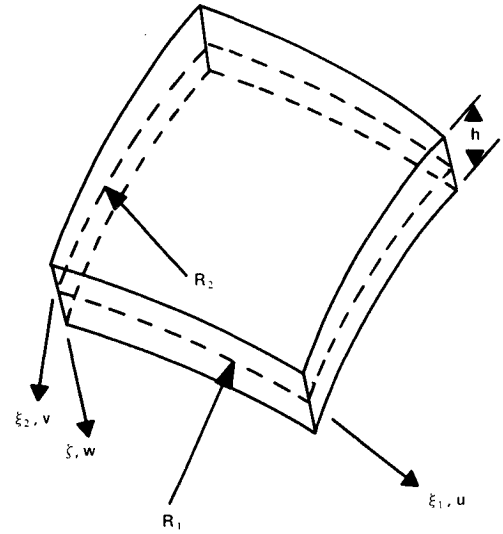

Fig. 1 Shell geometry described by orthogonal midsurface coordinates, ξ_1, ξ_2, and ζ.

Presented as Paper 89-1398 at the AIAA/ASME/ASCE/AHS/ASC 30th Structures, Structural Dynamics, and Materials Conference, Mobile, AL, April 3-5, 1989, received Jan. 25, 1989; revision received June 15, 1989. This paper is declared a work of the U.S. Government and is not subject to copyright in the United States.

*Assistant Professor, Engineering Mechanics, U.S. Air Force Academy, CO. Member AIAA.

†Professor, Aeronautics and Astronautics, Air Force Institute of Technology, Wright-Patterson AFB, OH. Associate Fellow AIAA.

where the transverse shears are zero on the lateral surfaces and are parabolic through the shell thickness. (Reddy and Liu[23] derive identical general shell kinematics as shown here but use Sanders shell relations.)

$$u_1(\xi_1,\xi_2,\zeta)=u(1-\zeta/R_1)+\zeta\psi_1+\zeta^3 k\left(\psi_1+\frac{w_{,1}}{\alpha_1}\right) \tag{1a}$$

$$u_2(\xi_1,\xi_2,\zeta)=v(1-\zeta/R_2)+\zeta\psi_2+\zeta^3 k\left(\psi_1+\frac{w_{,2}}{\alpha_2}\right) \tag{1b}$$

$$u_3(\xi_1,\xi_2)=w \tag{1c}$$

where $k=-4/3h^2$; u, v, w, ψ_γ ($\gamma=1,2$) are functions of midsurface shell coordinates ξ_γ; ψ_γ are bending rotations of the midsurface normals; $(\ )_{,\gamma}$ refers to differentiation with respect to ξ_γ; and α_γ are square roots of elements of the surface metric.

Strain-Displacement Relations

The strains are next found via the Green's strain-displacement relations where, again, exact nonlinear expression represent the in-plane strains but only the linear displacement terms are retained for the transverse strains, see Eq. (2). The in-plane strains, ϵ_1, ϵ_2, and ϵ_6, contain algebraically complicated nonlinear terms in displacement (ϵ_i^0 and κ_{ip}) that are functions of surface parameters ξ_1 and ξ_2. On the other hand, the transverse strains, ϵ_4 and ϵ_5, are linear with respect to displacement and have simple expressions. Each of the strain components, ϵ_i^0 and κ_{ip} of Eq. (2), are specialized for cylindrical coordinates and shown in Ref. 18.

$$\epsilon_i=\epsilon_i^0+\zeta^p\kappa_{ip} \qquad \begin{matrix} i=1,2,6 \\ p=\text{sum 1 to 7}\end{matrix} \tag{2a}$$

$$\epsilon_4=\left(\frac{w_{,2}}{\alpha_2}+\psi_2\right)(1+3k\zeta^2) \tag{2b}$$

$$\epsilon_5=\left(\frac{w_{,1}}{\alpha_1}+\psi_1\right)(1+3k\zeta^2) \tag{2c}$$

Potential Energy

We consider materials characterized by unidirectional fibers embedded in a matrix, i.e., transversely isotropic materials. The shell is composed of layers of this material where each layer is arbitrarily oriented, and therefore, the constitutive relations in material axes are transformed into shell midsurface coordinate axes as shown below in Eq. (3).

$$\begin{Bmatrix}\sigma_1\\ \sigma_2\\ \sigma_6\end{Bmatrix}^k=\begin{bmatrix}\bar{Q}_{11} & \bar{Q}_{12} & \bar{Q}_{16}\\ & \bar{Q}_{22} & \bar{Q}_{26}\\ & & \bar{Q}_{66}\end{bmatrix}^k\begin{Bmatrix}\epsilon_1\\ \epsilon_2\\ \epsilon_6\end{Bmatrix} \tag{3a}$$

$$\begin{Bmatrix}\sigma_4\\ \sigma_5\end{Bmatrix}^k=\begin{bmatrix}\bar{Q}_{44} & \bar{Q}_{45}\\ & \bar{Q}_{55}\end{bmatrix}^k\begin{Bmatrix}\epsilon_4\\ \epsilon_5\end{Bmatrix} \tag{3b}$$

where the $\bar{Q}_{ij}$ ($i,j=1,2,6$) and $\bar{Q}_{mn}$ ($m,n=4,5$) are elements of symmetric arrays of transformed stiffnesses for the kth ply, and σ_N and ϵ_N are measured with respect to shell coordinates ξ_α ($\alpha=1,2$) and ζ.[18] The σ_N are elements of the second Piola-Kirchhoff stress tensor.

The total potential energy of the shell Π_p is given in Eq. (4), where V represents the work done by external forces. Equation (4) indicates the complexity of the strain energy of the shell showing it to be comprised of many squares of the strain components, ϵ_i^0 and κ_{ip}, due to summations on up to four different indices. The potential energy is then written in terms of an area integral representing the shell midsurface in Eq. (5), where the ζ dependence has been integrated by defining a series of elasticity arrays shown in Eq. (6). In linear analyses, the elements from L, P, R, S, and T do not appear in Π_p since they are strictly a result of the assumed nonlinearity. Additionally, for symmetrically arranged laminates, the elements of the elasticity arrays associated with odd powers of ζ are identically zero since, in the present case, the middle surface, i.e., the reference surface, is also the plane of symmetry.

$$\Pi_p=\frac{1}{2}\int_\Omega\int_h \{\epsilon_j^0\,\epsilon_i^0\,\bar{Q}_{ij}+2\epsilon_j^0\,\bar{Q}_{ij}\kappa_{ip}\,\zeta^p+\kappa_{jp}\kappa_{ir}\bar{Q}_{ij}\,\zeta^{p+r} + \epsilon_m^0\epsilon_n^0\bar{Q}_{mn}+2\epsilon_n^0\kappa_{m2}\bar{Q}_{mn}\zeta^2+\kappa_{n2}\kappa_{m2}\bar{Q}_{mn}\zeta^4\,d\zeta\}d\Omega+V \tag{4}$$

where $i,j=1,2,6$; $p,r=$ sum 1 to 7; $m,n=4,5$; $\Omega=$ shell midsurface; and $\epsilon_4^0=w_{,2}/\alpha_2+\psi_2$, $\epsilon_5^0=w_{,1}/\alpha_1+\psi_1$, $\kappa_{42}=3k\epsilon_4^0$, $\kappa_{52}=3k\epsilon_5^0$

$$\begin{aligned}\Pi_p=\frac{1}{2}\int_\Omega\{&\epsilon_j^0\epsilon_i^0A_{ij}+2\epsilon_j^0(\kappa_{i1}B_{ij}+\kappa_{i2}D_{ij}+\kappa_{i3}E_{ij}+\kappa_{i4}F_{ij}\\ &+\kappa_{i5}G_{ij}+\kappa_{i6}H_{ij}+\kappa_{i7}I_{ij})+\kappa_{j1}\kappa_{i1}D_{ij}+2\kappa_{j1}\kappa_{i2}E_{ij}\\ &+(2\kappa_{j1}\kappa_{i3}+\kappa_{j2}\kappa_{i2})F_{ij}+2(\kappa_{j1}\kappa_{i4}+\kappa_{j2}\kappa_{i3})G_{ij}+(2\kappa_{j1}\kappa_{i5}\\ &+2\kappa_{j2}\kappa_{i4})H_{ij}+2(\kappa_{j1}\kappa_{i6}+\kappa_{j2}\kappa_{i5}+\kappa_{j3}\kappa_{i4})I_{ij}+(2\kappa_{j1}\kappa_{i7}\\ &+2\kappa_{j2}\kappa_{i6}+2\kappa_{j3}\kappa_{i5}+\kappa_{j4}\kappa_{i4})J_{ij}+2(\kappa_{j2}\kappa_{i7}+\kappa_{j3}\kappa_{i6}\\ &+\kappa_{j4}\kappa_{i5})K_{ij}+(2\kappa_{j3}\kappa_{i7}+2\kappa_{j4}\kappa_{i6}+\kappa_{j5}\kappa_{i5})L_{ij}+2(\kappa_{j4}\kappa_{i7}\\ &+\kappa_{j5}\kappa_{i6})P_{ij}+(2\kappa_{j5}\kappa_{i7}+\kappa_{j6}\kappa_{i6})R_{ij}+2\kappa_{j6}\kappa_{i7}S_{ij}+\kappa_{j7}\kappa_{i7}T_{ij}\\ &+\epsilon_m^0\epsilon_n^0A_{mn}+2\epsilon_n^0\kappa_{m2}D_{mn}+\kappa_{n2}\kappa_{m2}F_{mn}\}\,d\Omega+V\end{aligned} \tag{5}$$

$$[A_{ij},B_{ij},D_{ij},E_{ij},F_{ij},G_{ij},H_{ij},I_{ij},J_{ij},K_{ij},L_{ij},P_{ij},R_{ij},S_{ij},T_{ij},]=\int_h\bar{Q}_{ij}\,[1,\zeta,\zeta^2,\zeta^3,\zeta^4,\zeta^5,\zeta^6,\zeta^7,\zeta^8,\zeta^9,\zeta^{10},\zeta^{11},\zeta^{12},\zeta^{13},\zeta^{14}]\,d\zeta \tag{6a}$$

$$[A_{mn},D_{mn},F_{mn}]=\int_h\bar{Q}_{mn}\,[1,\zeta^2,\zeta^4]\,d\zeta \tag{6b}$$

III. Finite-Element Solution

The shell domain is discretized such that the continuum displacements are approximated by nodal values and interpolation functions. The displacement gradient vector $\boldsymbol{d}$ is defined based on the unique displacement terms of the strain-displacement relations. As seen in Ref. 18, $\boldsymbol{d}$ is an 18×1 array given in Eq. (7) and Eq. (8) shows the relationship between $\boldsymbol{d}$ and the vector of nodal displacement unknowns q.

$$\boldsymbol{d}^T=\{u\ u_{,1}\ u_{,2}\ v\ v_{,1}\ v_{,2}\ w\ w_{,1}\ w_{,2}\ w_{,11}\ w_{,22}\ w_{,12}\ \psi_1\ \psi_{1,1}\ \psi_{1,2}\ \psi_2\ \psi_{2,1}\ \psi_{2,2}\} \tag{7}$$

$$\boldsymbol{d}=\mathfrak{D}q \tag{8}$$

where $\mathfrak{D}$ is an array of interpolation functions and their derivatives.

The potential energy is then given for the discretized domain in Eq. (9). The first variation of the energy, $\delta\Pi_p$, gives the equilibrium equations $F(q)$, also shown in Eq. (9). The symmetric 18×18 arrays K, N_1, and N_2 were defined from Eq. (5) using a generalization of the approach described by Rajasekaran and Murray.[24]

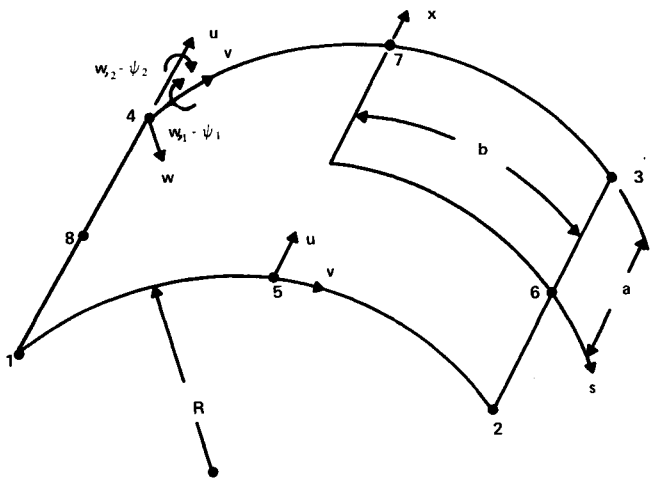

Fig. 2 36-DOF rectangular shell element. Corner nodes have 7 DOF, and midside nodes have 2 DOF. Cylindrical axes *x-s* result from specialization of $\xi_1 - \xi_2$ expressions, respectively.

$$\Pi_p = \frac{q^T}{2} \int_\Omega \mathfrak{D}^T \left[K + \frac{N_1}{3} + \frac{N_2}{6} \right] \mathfrak{D} \, d\Omega q - q^T R$$

$$\delta\Pi_p = \delta q^T \int_\Omega \mathfrak{D}^T \left[K + \frac{N_1}{2} + \frac{N_2}{3} \right] \mathfrak{D} \, d\Omega q - \delta q^T R$$

$$= \delta q^T F(q) = 0 \tag{9}$$

where R is a column array of the nodal loads, K is an array of constant stiffness coefficients, N_1 is an array of stiffness coefficients that are linear in displacement, and N_2 is an array of stiffness coefficients that are quadratic in displacement.

A rectangular eight-noded curved element has been developed for cylindrical shells by specializing the above equations for a cylindrical midsurface; see Fig. 2. The element has 36 degrees of freedom (DOF) and assumes quadratic distributions for the in-plane displacements u and v, and linear distributions for the bending rotations ψ_α. The remaining nodal DOF, w and its two first derivatives, are interpolated by nonconforming cubic-shape functions. Although a nonconforming element results, it will pass the patch test and therefore converges as the mesh is refined. However, monotonic convergence from a stiffer solution can no longer be expected. Generally shaped quadrilateral elements pass a "milder" form of the patch test but convergence is of a lower order. The elemental interpolations described above represent a simple, straight-forward application of finite-element principles for the present Π_p. As a consequence of these interpolations, exact integration of the elemental stiffnesses requires 7×7 uniform Gauss integration. However, a uniform 5×5 scheme proved to be much more economical without loss of accuracy, and hence, was used instead.[25,26]

Solutions to the nonlinear equations of Eq. (9) are found via a Newton-Raphson approach. Equation (9) is linearized by a truncated Taylor-series expansion resulting in the incremental/iterative equations shown in Eq. (10). A simple displacement control algorithm allows solutions beyond collapse points.

Generally, in a large rotation formulation, the applied loads develop higher-order nonlinear terms. Instead of including these terms in Π_p, solutions presented herein result from prescribing displacement and then the corresponding equilibrium loads are calculated.

$$\int_\Omega \mathfrak{D}^T \left[K + N_1 + N_2 \right] \mathfrak{D} \, d\Omega \Delta q = -F(q) \tag{10}$$

A more detailed account of the theory and subsequent finite-element casting will appear in Ref. 27.

IV. Validation of Approach

The approach is verified by comparing present results to those due to Sabir and Lock[28] who analytically trace the equilibrium path of an isotropic cylindrical panel subjected to a center transverse point load. A 4×6 mesh (longitudinal by circumferential) modeled one quadrant of the panel. Figure 3 shows the transverse response of the center of the panel due to the point load. As can be seen, the present approach duplicates the referenced results beyond collapse.

V. Cylindrical Quasi-isotropic Shell Panel with Cutout

The theory is next applied to the shell geometry of Fig. 4. This type of structure might be found on the fuselage of an aircraft, for example, and the nonlinear response of the structure as it is axially compressed is of interest. The theoretical results are compared to the experimental findings of Tisler.[11]

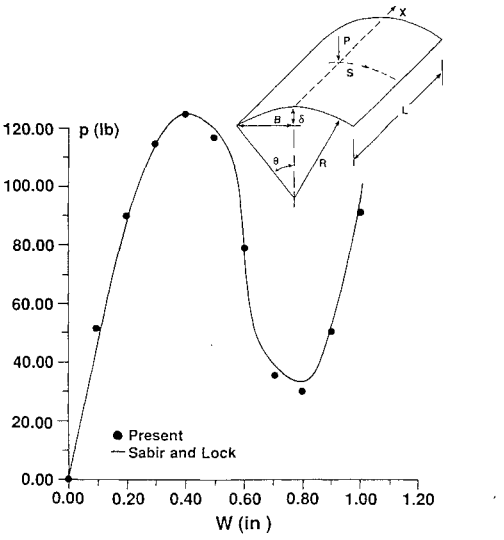

Fig. 3 Point loaded isotropic cylindrical shell panel response ($E = 4.5e6$, $\nu = 0.3$, $R = 100$ in., $h = 0.5$ in., $L = 20$ in., $\theta = 0.1$ rad, $\delta/B = 0.05$, longitudinal edges hinged, circumferential edges free).

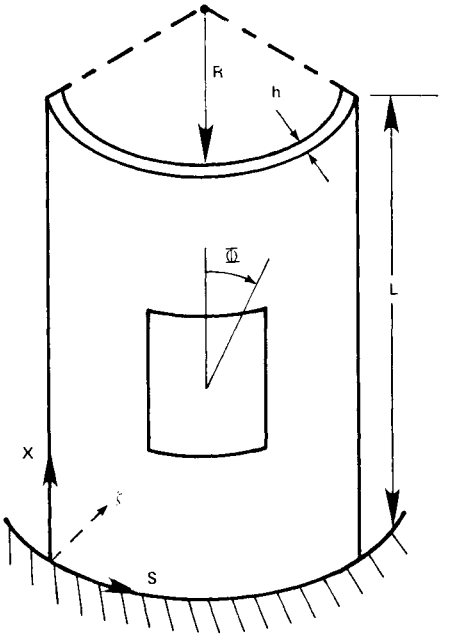

Fig. 4 $[0/\pm 45/90]_s$ panel geometry showing square 4×4-in. cutout. Ply orientation angle Φ; L, R, arclength = 12 in.; $h = 0.039$ in.; midsurface displacements u, v, w correspond to coordinate axes, x, s, ζ, respectively.

Tisler also analytically determined the panel response using a commercially available finite-element package. He found good agreement between analytical and experimental panel equilibrium paths except for the panels with a larger cutout, i.e., greater than 2×2 in. The analytical response for panels with a 4×4 in. cutout (Fig. 4) was more flexible than the experimental response even when assuming overly constrained boundary conditions in the analytical model. This disagrees with the expected stiffer analytical response resulting from the displacement-based finite-element formulation that he used. Experimental local rotations on the panel with a 4×4-in. cutout were approximately 10 deg, thus perhaps exceeding the intermediate nonlinear capabilities of the specific finite element used and at least partially explaining his differences from the experiment. These conclusions are consistent with similar findings of axially compressed composite panels with larger circular holes investigated by Knight and Starnes.[4] We, therefore, attempt to analytically predict the panel response using the present simplified large rotational approach.

The orthotropic material properties (Hercules 3501 graphite epoxy) of the panels tested by Tisler are given in Eq. (11). The boundary conditions have the bottom edge, i.e., $x = 0$, completely clamped; see Fig. 4. The top edge is clamped as well, only the axial displacement u is prescribed since the analytical load is input by a uniform axial displacement along the top edge ($x = 12$ in). As discussed by Tisler,[11,14] the uniform displacement loading better resembles the actual test apparatus and, additionally, he found that the distinction between uniform displacement and uniform loading along the top edge is very important for the panels with a larger cutout. The boundary conditions for the vertical edges are simple; however, posttest inspection of the panels showed evidence that the circumferential displacement v along these edges was not totally free as was originally thought. Therefore, the present analytical results will reflect two set of boundary conditions for the vertical edges where the circumferential displacement v is free or fixed. The boundary conditions are shown in Eq. (12).

$$E_1 = 18.844 \times 10^6 \text{ psi} \tag{11a}$$

$$E_2 = 1.468 \times 10^6 \text{ psi} \tag{11b}$$

$$G_{12} = G_{13} = 0.91 \times 10^6 \text{ psi} \tag{11c}$$

$$G_{23} = 0.45 \times 10^6 \text{ psi} \tag{11d}$$

$$\nu_{12} = 0.28 \tag{11e}$$

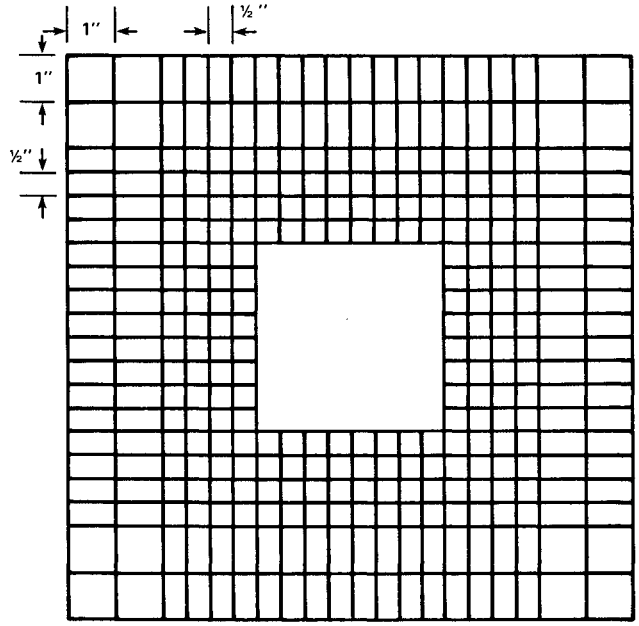

Fig. 5 20 × 20 mesh for cylindrical panel with 4 × 4-in. cutout.

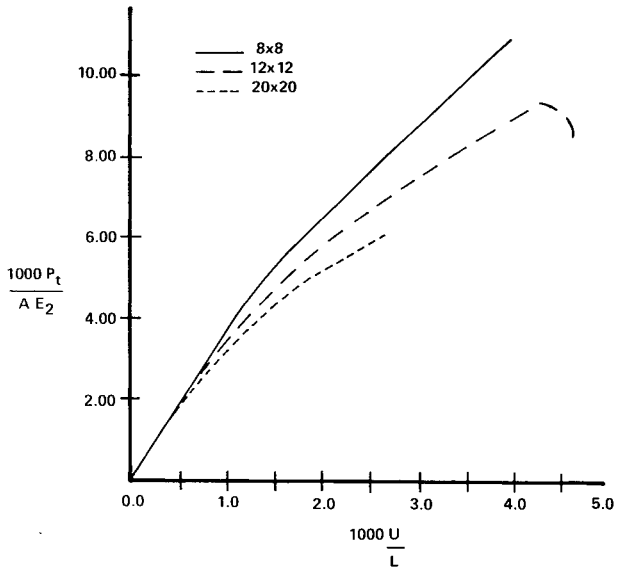

Fig. 6 Panel with 4 × 4-in. cutout nonlinear analysis ($h = 0.039$, v fixed, P_t = total top edge axial force, $A = 12h$).

Along $x = 0$:

$$u = v = w_{,1} = w_{,2} = \psi_1 = \psi_2 = 0 \tag{12a}$$

Along $x = 12$:

$$v = w = w_{,1} = w_{,2} = \psi_1 = \psi_2 = 0 \tag{12b}$$

Along $s = 0$, 12:

$$v = w = w_{,1} = \psi_1 = 0 \ (v \text{ fixed}) \tag{12c}$$

or

$$w = w_{,1} = \psi_1 = 0 \ (v \text{ free}) \tag{12d}$$

Initial model validation was based on linear analyses of several mesh arrangements of the 36 DOF element both with and without the cutout. Figure 5 shows the final of three progressively more refined mesh arrangements for the shell midsurface planform where, although not shown, elements are actually present within the center square cutout. To model a 4×4-in. cutout, no stiffness is calculated for those elements within the cutout region. This is done so that an automatic mesh generator can be used. Additionally, the nodes of those elements within the cutout not on the cutout border must be constrained. Calculations were performed on a Cyber 845 digital computer.

When the actual panels were cut, care was taken to ensure that the corners of the cutout were rounded. In this way, large stress concentrations would not form at the corners as the panels were experimentally loaded. Therefore, although the cutout corners of the analytical model are sharp, mesh refinement is not as severe as that required for a singularity. By keeping the mesh refinement relatively coarse, an analytical

Table 1 Total top edge compressive force from linear analysis ($1000\,u/L = 0.8333$)

Mesh	$1000P_t/AE_2$ No cutout	4-in. cutout
8×8	4.340	3.173
12×12	4.323	3.082
20×20	4.323	3.064

[a]Circumferential displacement v fixed along vertical edges. $h = 0.045$ in. P_t = total top edge axial force. $A = 12h$.

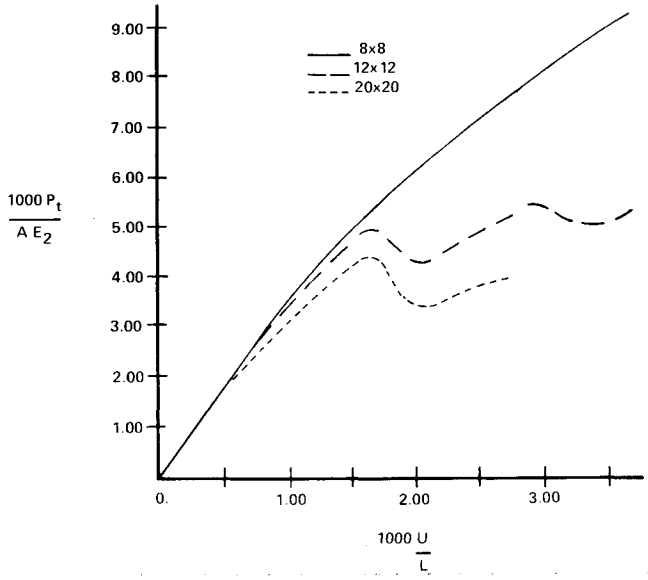

Fig. 7 4×4-in. cutout panel nonlinear analysis ($h = 0.039$, v free, P_t = total top edge axial force, $A = 12h$).

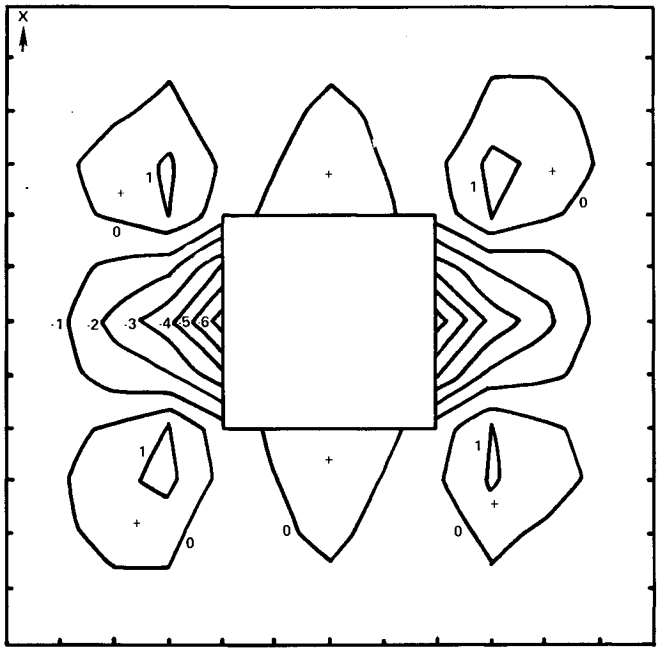

Fig. 8 Panel planform contour plot of radial displacement w/h.

stress singularity cannot develop, hence representing the actual panels more accurately.

The results of the linear analysis for a prescribed compressive axial displacement along the top edge of $u = 0.010$ in. ($1000u/L = 0.8333$) are shown in the Table 1 for panels with and without the 4 × 4-in. cutout. For each mesh, the total nondimensionalized top edge axial force $\bar{P}$ is shown. Note that the cutout gives a significantly more flexible panel. The linear results show that the 20 × 20 mesh results represent converged solutions. This mesh arrangement is used in the nonlinear collapse studies as well and is identical to that used in Refs. 9 and 11. A further refinement was not tested because the 20 × 20 mesh already resulted in a large nonlinear problem (3074 active DOF) and thus, only a limited number of 20 × 20 analyses were performed.

A homogeneous panel, i.e., one with no cutout, of the same dimensions and material as in Fig. 4, was analytically tested in axial compression and compared to known experimental results. This served as verification of the nonlinear model prior to the analysis of the panels with cutouts. This initial study shows that the present formulation does not require a geometric imperfection to "trigger" the nonlinear response. Apparently, other formulations do not have adequate displacement coupling between the in-plane and transverse displacements and therefore, to achieve collapse in perfect panels that are axially compressed, a numerical imperfection with a small transverse amplitude must be assumed.[3] To measure its effect in this analysis, a small transverse point load was applied at the panel center such that a small amplitude imperfection resulted throughout the panel. This had a negligible effect on the results.

Upon verification of the model, nonlinear collapse of the panels with the cutout was studied. The global nonlinear re-

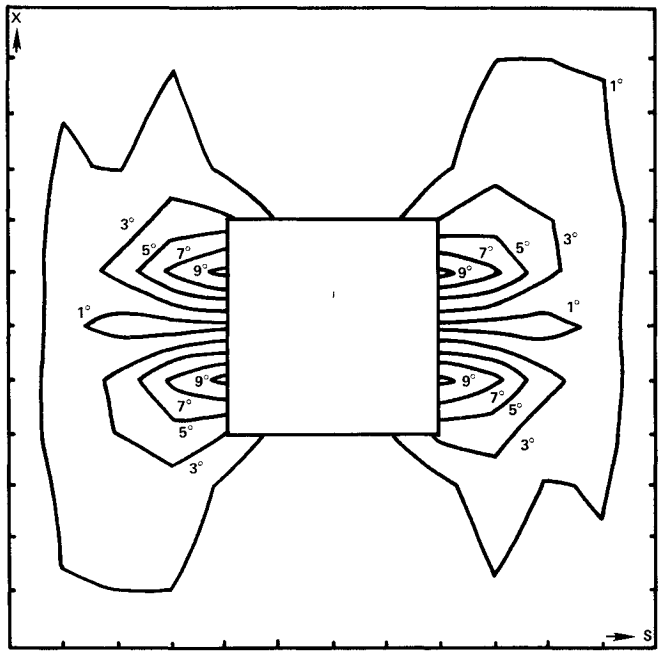

Fig. 9 Panel planform contour plot of bending rotation $|\psi_1|$ (deg).

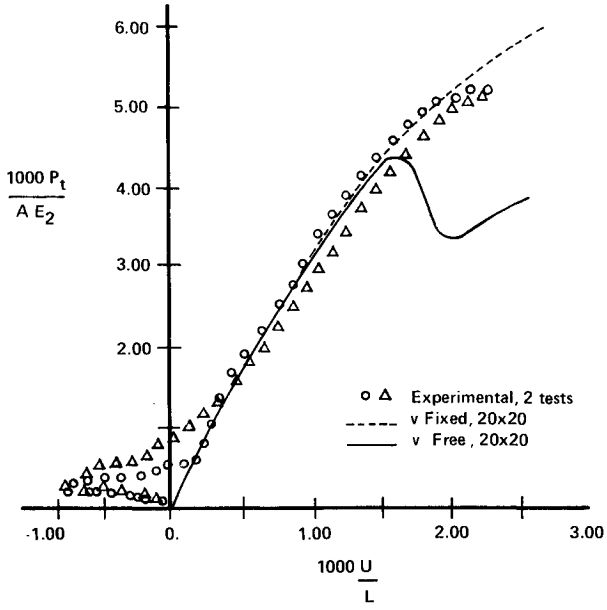

Fig. 10 Global panel response, nondimensionalized compressive displacement vs nondimensionalized load ($h = 0.039$, P_t = total top edge load, $A = 12h$).

sponse of the panel is indicated by the equilibrium path of nondimensionalized top edge axial displacement vs nondimensionalized total edge axial load. The results for the 20×20 mesh of Fig. 5 are shown in Figs. 6 and 7. Figures 6 and 7 are those results obtained when the circumferential displacement v is fixed and free, respectively. In Fig. 6, the 12×12 mesh nondimensionalized collapse load is $\bar{P} = 9.428$ ($P_t = 6477$ lb). The 20×20 mesh result had not yet collapsed for the largest axial compressive displacement shown. However, the results show that it should collapse for a $\bar{P}$ less than approximately 7.300 ($P_t = 5000$ lb) based on a crude extrapolation and the 12×12 mesh results. In Fig. 7, the 12×12 mesh collapses at $\bar{P} = 4.990$ ($P_t = 3428$ lb) for no v restraint along the vertical edges. The load then starts to increase again resulting in a second collapse at $\bar{P} = 5.489$ ($P_t = 3771$ lbs). The two humped behavior of the 12×12 mesh in Fig. 7 has been similarly reported by Knight and Starnes.[4] The 20×20 mesh shows a collapse load of $\bar{P} = 4.450$ ($P_t = 3057$ lb). Figures 6 and 7 show that the circumferential displacement boundary condition has a fairly significant influence on the collapse load.

Figures 8 and 9 show contour plots of nondimensionalized radial displacement w/h and bending rotations ψ_1 (deg) for the panel planform from the v fixed, 20×20 mesh analysis for $\bar{P} = 6.10$ ($P_t = 4194$ lb). As seen, both large displacements ($w/h > 6$) and large rotations ($\psi_1 > 9$ deg) are occuring near the vertical edges of the cutout. For these regions, the panel is bowing outward, i.e., away from center of curvature, whereas the regions of the panel near the horizontal edges of the cutout are bowing inward. This is consistent with experimental observations. The analytical results for the above case also indicate relatively small shear rotations throughout the panel with maximum values of about 0.2 deg occurring near the simply supported vertical edges. Although the shear rotations are small when compared to the bending rotations, they contribute to the overall flexibility of the panel and therefore may be important degrees of freedom in determining the global response of the panel.

A final comparison is presented comparing Tisler experimental data and the present analytical results using the 20×20 mesh. The experimental results shown in the figures represent linear variable differential transducer (LVDT) data taken

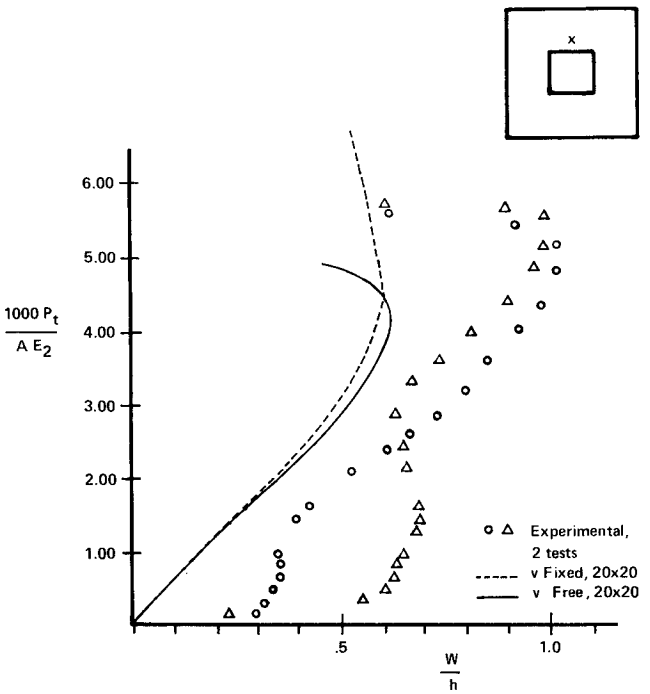

Fig. 11 Local panel response, nondimensionalized radial displacement vs nondimensionalized load for point shown, ½″ above cutout edge ($h = 0.039$, P_t = total top edge load, $A = 12h$).

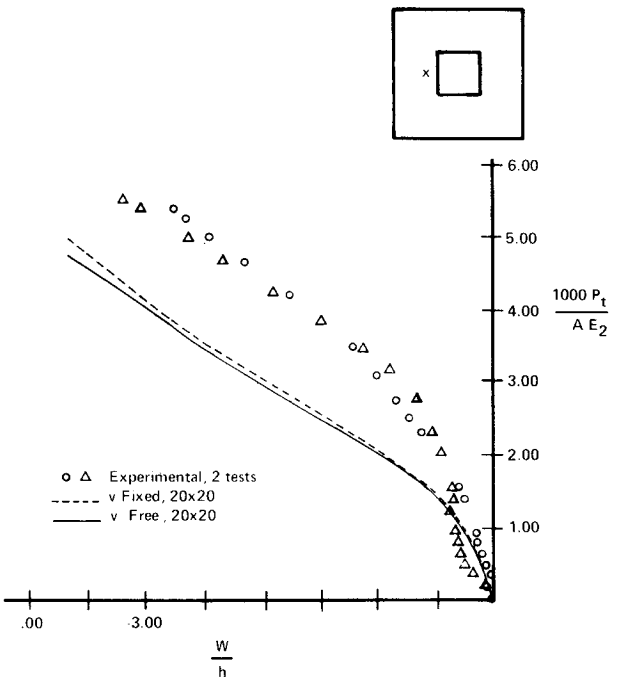

Fig. 12 Local panel response, nondimensionalized radial displacement vs nondimensionalized load for point shown, ½″ left of cutout edge ($h = 0.039$, P_t = total top edge load, $A = 12h$).

from two panel tests. Figure 10 gives the global panel response of nondimensionalized top edge axial displacement vs total top edge axial load. This figure shows an unusual experimental equilibrium path for axial loads less than approximately $\bar{P} = 1.164$ ($P_t = 800$ lb). For these loads, the LVDT that measured the panel axial compression as the load was applied was reading tension. Wilder,[29] who used the same test apparatus in a study of panel delaminations, discovered that this anomaly was due to an improper attachment of the panel to the loading structure. For loads above 800 lb, however, the panel is properly seated and the data is assumed to be valid.

Also plotted in Fig. 10 are the analytical results from the present formulation. As can be seen, the experimental panel-collapse values of approximately $\bar{P} = 5.00$ ($P_t \cong 3500$ lb) fall between the two analytical predictions. The panel with v free along the vertical edges predicts a smaller collapse load than the experimental and when v is fixed, the collapse is higher than the experimental. This would indicate that the actual panels were neither fully restrained nor fully free during loading and therefore some movement was permitted. This is consistent with the experimental observations made by Tisler.

Analytical and experimental results for the local behavior of the panel are also compared in Figs. 11 and 12. Load-displacement curves are given for the nondimensionalized *radial* displacement w/h at two points near the cutout edge; see figures. In the figures, the comparisons for small values of axial load are poor. However, the comparisons for loads above approximately $\bar{P} = 1.164$ ($P_t = 800$ lb) are quite good considering that we are examining very localized panel behavior. Except for an initial shift in the experimental data in both figures, both of the analytical curves match the experimental trends. This shift in the data may be related to the panel-seating problem mentioned earlier.

VI. Conclusions

A shell theory that includes parabolic transverse shear and allows large rotations is applied to an axially compressed quasiisotropic cylindrical panel with a cutout. The finite-element results show good agreement with experimental results for both global and local panel response. The analytical results give the expected large rotations near the panel cutout edges

but indicate small values of transverse shear rotations throughout the panel.

Acknowledgment

This work was supported in part by AFOSR Grant PD880010.

References

[1]Sobel, L. H., Weller, T., and Agarwal, B. L., "Buckling of Cylindrical Panels under Axial Compression," *Computers and Structures*, Vol. 6, 1976, pp. 29–35.

[2]Bauld, N. R., and Satyamurthy, K., "Collapse Load Analysis for Plates and Shells," Air Force Flight Dynamics Lab., Wright-Patterson AFB, OH, AFFDL-TR-79-3038, 1979.

[3]Becker, M. L., Palazotto, A. N., Khot, N. S., "Instability of Composite Panels," *Journal of Aircraft*, Vol. 18, Sept. 1981, pp. 739–743.

[4]Knight, N. F., and Starnes, J. H., "Postbuckling Behavior of Axially Compressed Graphite Epoxy Cylindrical Panels with Circular Holes," *Collapase Analysis of Structures*, PVP Vol. 84, edited by L. H. Sobel, ASME, 1984, pp. 153–167.

[5]Hebert, J. S., and Palazotto, A. N., "Comparison between Experimental and Numerical Buckling of Curved Cylindrical Composite Panels," *Proceedings of the 12th Southeastern Conference on Theoretical and Applied Mechanics*, Auburn University, 1984, pp. 124–129.

[6]Janisse, T. C., and Palazotto, A. N., "Collapse Analysis of Composite Cylindrical Panels with Small Cutouts," *Journal of Aircraft*, Vol. 21, No. 9, 1984, pp. 731–733.

[7]Whitney, J. M., "Buckling of Anisotropic Laminated Cylindrical Plates," *AIAA Journal*, Vol. 22, No. 11, 1984, pp. 1641–1645.

[8]Leissa, A. W., *Buckling of Laminated Composite Plates and Shell Panels*, Wright-Patterson AFB, OH, AFWAL-TR-85-3069, 1985.

[9]Lee, C. E., and Palazotto, A. N., "Collapse Analysis of Composite Cylindrical Panels with Small Cutouts," *Journal of Composite Structures*, Vol. 4, 1985, pp. 217–219.

[10]Bushnell, D., "Static Collapse: A Study of Methods and Modes of Behavior," *Finite Elements in Analysis and Design*, Vol. 1, 1985.

[11]Tisler, T. W., "Collapse Analysis of Cylindrical Composite Panels with Large Cutouts under an Axial Load," M.S. Thesis, GA/MS/86D-1, School of Engineering, Air Force Inst. of Technology (AU), Wright-Patterson AFB, OH, 1986.

[12]Hermsen, M. F., and Palazotto, A. N., "The Effects of Cutout Location and Material Degradation on the Collapse of Composite Cylindrical Panels," *Nonlinear Analysis and NDE of Composite Material Vessels and Components*, Vol. 115, edited by D. Hui, J. Duke, and H. Chung, ASME 1986, pp. 43–57.

[13]Horban, B. A., and Palazotto, A. N., "The Experimental Buckling of Cylindrical Composite Panels with Eccentrically Located Circular Delaminations," *Journal of Spacecraft and Rockets*, Vol. 24, No. 4, AIAA, Washington, D.C., July–Aug., 1987, pp. 349–352.

[14]Palazotto, A. N., Tisler, T. W., "Considerations of Cutouts in Composite Cylindrical Panels," *Computers and Structures*, Vol. 29, 1988, pp. 1101–1110.

[15]Knight, N. F., Starnes, J. H., "Postbuckling Behavior of Selected Curved Stiffened Graphite-Epoxy Panels Loaded in Axial Compression," *AIAA Journal*, Vol. 26, No. 3, 1988, p. 344–352.

[16]Reddy, J. N., "A Simple Higher-Order Theory for Laminated Composite Plates," *Journal of Applied Mechanics*, Vol. 51, Dec. 1984, pp. 745–752.

[17]Librescu, L., "Refined Geometrically Nonlinear Theories of Anisotropic Laminated Shells," *Quarterly Journal of Applied Mathematics*, Vol. 45, April 1987, pp. 1–22.

[18]Dennis, S. T., and Palazotto, A. N., "Transverse Shear Deformation in Orthotropic Cylindrical Pressure Vessels Using a Higher-Order Shear Theory," *AIAA Journal* Vol. 27, No. 10, 1989, pp. 1441–1447.

[19]Koiter, W. T., "A Consistent First Approximation in the General Theory of Thin Elastic Shells," *Proceedings of the Symposium on Theory of Thin Elastic Shells*, Amsterdam, North Holland, 1960, pp. 12–33.

[20]John, F., "Estimates for the Derivatives of the Stresses in a Thin Shell and Interior Shell Equations," *Communications on Pure and Applied Mathematics*, Vol. XVIII, May 1965, pp. 235–267.

[21]Pagno, N. J., "Exact Solutions for Laminated Cylindrical Shells in Cylindrical Bending," *Journal of Composite Materials*, Vol. 3, July 1969, pp. 398–411.

[22]Ren, J. G., "Exact Solutions for Laminated Cylindrical Shells in Cylindrical Bending," *Composites Sciences and Technology*, Vol. 29, 1987, pp. 169–187.

[23]Reddy, J. N., and Liu, C. F., "A Higher-Order Shear Deformation Theory of Laminated Elastic Shells," *International Journal of Engineering Science*, Vol. 23, No. 3, 1985, pp. 319–330.

[24]Rajasekaran, S., and Murray, D. W., "Incremental Finite-Element Matrices," *Journal of Structure Engineering, Structural Division*, American Society of Civil Engineers, 1973, pp. 2423–2437.

[25]Gallagher, R. H., *Finite Element Analysis Fundamentals*, Prentice Hall, Englewood Cliffs, NJ, 1975.

[26]Walz, J. E., Fulton, R. E., and Cyrus, N. J., "Accuracy and Convergence of Finite-Element Approximations," Air Force Flight Dynamics Labs., Wright-Patterson AFB, OH, AFFDL-TR-68-150, 1968.

[27]Dennis, S. T., and Palazotto, A. N., "Large Displacement and Rotational Formulation for Laminated Shells Including Parabolic Transverse Shear," *International Journal of Nonlinear Mechanics* (to be published).

[28]Sabir, A. B., and Lock, A. C., "The Application of Finite Elements to the Large Deflection Geometrically Nonlinear Behaviour of Cylindrical Shells," *Variational Methods in Engineering*, edited by C. A., Brebbia and H. Tottenham, University Press, Southhampton, 1972, pp. 766–775.

[29]Wilder, B. L., "A Study of Damage Tolerance in Curved Composite Panels," M.S. Thesis, AFIT/GA/AA/88M-2, Wright Patterson AFB, OH, 1988.